Hindawi
Advances in Civil Engineering
Volume 2020, Article ID 8869810, 19 pages
https://doi.org/10.1155/2020/8869810

Research Article

Structural Damage Identification Based on the Wavelet Transform and Improved Particle Swarm Optimization Algorithm

Jia Guo, Deqing Guan, and Jianwei Zhao

Department of Civil Engineering, Changsha University of Science & Technology, Changsha, Hunan, China

Correspondence should be addressed to Deqing Guan; 491596452@qq.com

Received 8 April 2020; Revised 18 June 2020; Accepted 23 July 2020; Published 8 August 2020

Academic Editor: Dongsheng Li

A method based on the wavelet transform and improved particle swarm optimization (WIPSO) algorithm is proposed to identify the microdamage of structures. First, the singularity of wavelet coefficients is used to identify the structural damage location, and then, the improved particle swarm optimization (IPSO) algorithm is used to calculate the optimal solution of the objective function of the structural damage location to determine the structural damage severity. To study the performance of WIPSO, the structural microdamage severity is set within 10%, and a numerical simulation and experimental structure under different damage scenarios are considered. In addition, the ability of wavelet coefficients to identify the location of the structural damage under different noise levels is studied. To evaluate the performance of IPSO, the standard particle swarm optimization algorithm with an inertia weight factor of 0.8 (0.8PSO), the genetic algorithm (GA), and the bat algorithm (BA) are also considered. The results show that WIPSO can effectively and accurately identify the structural damage location and severity. Wavelet transform is very robust to the structural damage location. Compared with the standard 0.8PSO and other mainstream algorithms, IPSO has good convergence and performs more stable and more accurate in the identification of structural damage severity.

1. Introduction

During the service life of a structure, microdamages occur, which are difficult for direct visual identification; these microdamages will accumulate and eventually lead to structure failure or even collapse. Therefore, research on structural microdamage has become increasingly urgent. Structural damage identification can not only evaluate whether the working state of a structure is safe but also provide a technical basis for structural reinforcement measures. In the investigation of large-scale structures, it is time- and labor-consuming to carry out nondestructive testing with visual inspection, and only part of the overall state information of a structure can be provided. However, damage identification based on structural vibration can be used to obtain complete structural information.

The basic theory of damage identification based on the vibration response is that the damage causes changes in physical properties, such as stiffness, damping, and mass; furthermore, the damage affects the modal characteristics, i.e., modal damping, mode shape, and natural frequency. Therefore, damage can be identified by analyzing changes in the structural vibration characteristics. In recent decades, experts and scholars in related fields used vibration responses as the basis for damage identification [1–4], and several approaches have been suggested [5, 6]. For example, based on the natural frequency, the modal strain energy damage identification method of the displacement mode can be used, and the effectiveness of the method for identifying the damage location of complex structures was verified by numerical simulation [7]. In addition, because it is difficult to accurately measure freedom of rotation, the measured displacement mode information was expanded to obtain this information [8]. The natural frequency and mode shape are global parameters, and the local damage sensitivity to global parameters is low; thus, it is still

difficult to use the natural frequency and mode shape to accurately locate and quantify damage. However, the strain mode has more information than the displacement mode.

In recent years, strain mode and displacement mode have been used to identify the structural damage, and research shows that the strain mode has stronger sensitivity to damage [9]. The curvature mode is affected by noise to some extent after the noise is added to the experiment data, but the strain mode can effectively avoid noise pollution [10]; therefore, a damage identification method with high accuracy and good noise resistance can be established based on the strain mode. At present, establishing a damage index is the main method of structural damage identification based on the strain mode, and the changes in the damage index before and after structural damage based on the strain mode are obtained to identify the damage. Both numerical simulation and experimental results demonstrate that the method of structural damage identification based on the strain mode can accurately identify the damage location, and the strain mode has better noise resistance than the displacement mode [11, 12].

Due to the poor effect of using the dynamic structural parameters to identify the microdamage, signal processing and related technologies are proposed to assist with damage identification. Fourier transform analysis functions from the time-based domain to the frequency-based domain are used, but they lack resolution in the time domain, which makes it difficult to extract local information. Effective signal processing in the time-frequency domain to achieve high-resolution analysis has always been a research hotspot and challenge in related fields [2, 13]. In recent years, many scholars have proposed various methods to solve the structural damage identification problem, but there are still some shortcomings. For example, the Hilbert–Huang transform can intuitively assess the structural damage by analyzing the natural mode function of the structural response signal and comparing the shape factors of the natural mode function of the response signal before and after damage [14]. However, the first IMF of the Hilbert–Huang transform may cover a wide frequency range, which will cause signal distortion and lead to errors [15]. To overcome these deficiencies, wavelet analysis was proposed because of its multiresolution analysis and good localization characteristics in the time-frequency domain. Wavelet analysis can effectively solve the resolution contradiction in the time-frequency domain and diagnose the vibration state of the structure, so it can be used for structural damage identification [16, 17].

With the development of wavelet analysis in various fields, the identification of the structural damage based on wavelet analysis is also developing. The singularity principle of wavelet analysis enables the experimental modal parameters of the structure to obtain singularity of the experimental data after wavelet transformation; therefore, the structural damage location can be identified, and the damage severity can be defined by the relevant damage index (such as the Lipschitz index) [18]. It is a common method to transform the dynamic characteristic parameters of structures into corresponding damage indexes by wavelet transform. As one of the most commonly used damage indexes, the wavelet coefficient can be used not only as an index to identify local anomalies [19] but also as a component of the damage index [20, 21]. The damage location can be directly reflected by a wavelet coefficient graph [22, 23], which makes the damage location more intuitive. In addition, wavelet transform is used to process the modal data of damaged structures, and the difference with the damage approximate function is calculated to obtain the structural damage location [24]. Similar methods have been studied, such as calculating the modal vector differences of a structure by wavelet transform and taking the accumulated value of the modal vector differences as the damage index to identify the structural damage location [25]. He et al. [26] used wavelet transform to decompose the changes in the frequency component of a moving load from the total dynamic displacement response to locate the suspected damage area. All of the above methods are based on wavelet transform, which has good resolution in the time-frequency domain.

Although wavelet analysis can efficiently and accurately identify the location of the structural damage, it cannot directly identify damage severity. Recently, intelligent optimization algorithms have been a research hotspot to identify damage severity. Some experts and scholars have tried to apply intelligent algorithms to structural damage identification. The artificial immune algorithm, GA, and other algorithms have been successfully applied to damage identification in conduit platforms and bridges [4, 27, 28], and these algorithms have achieved good damage identification. Moreover, GA has also been used to solve the multiobjective optimization problem, and it was found that the method for damage location and quantification has a good application prospect. Tiachacht et al. [29] proposed a method of structural damage identification and quantification based on the modified Cornwell indicator (MCI) and GA, and they successfully identified the damage of two-dimensional truss and three-dimensional frame structures by GA-MCI. Tran-Ngoc et al. [30] applied a particle swarm optimization (PSO) algorithm and genetic algorithm (GA) to update the parameters of the Nam O Bridge model. The result shows that PSO not only provides a better accuracy between the numerical model and measurements but also reduces the computational cost compared to GA. In addition, with the in-depth study of neural network training, it is found that neural networks have strong abilities for structural damage identification [31] and high sensitivity for local damage identification [32]. For the damage identification of plate-shaped structures, Guedria [33] introduced the accelerated differential evolution algorithm, constructed the objective function using the flexibility matrix, solved the problem of damage identification, and verified the results by numerical simulation. Nobahari et al. [34] combined the residual force vector and GA to accurately identify the damage location and severity of truss structures in two steps; the work of calculating the damage severity of GA can be effectively reduced after the residual force vector is used to identify the damage location. Chatterjee et al. [35] improved the accuracy of the traditional learning algorithm training artificial neural network to identify the structural damage through PSO optimization of the optimal weight of

the neural network selector. Zhao et al. [36] combined the tabu search method and chaos search method to optimize the artificial bee colony algorithm and improve the exploration and development ability of the algorithm. Through numerical simulation and testing, the method was proved to effectively identify the structural damage, and the method has good robustness when there are enough measurement data.

At present, scholars and research groups are trying to study how to combine wavelet analysis and intelligent algorithms to identify the location and severity of the structural damage. Dynamic parameter data of damaged structures can identify structural damage locations by wavelet transform [37], and the damage severity of the structures can be identified by intelligent algorithms [38]. The relevant case analysis combines wavelet analysis and intelligent algorithms to accurately identify the damage location and severity of the structure [39–41]. Through the damage identification of I-beams in relevant experiments, it is found that the method of damage location and severity identification of the I-beam in steel structures is divided into two steps that have high accuracy in theory and practice [42].

PSO originated from a biological mechanism and was proposed by Kennedy and Eberhard in 1995. PSO was originally used as an optimization technique for mathematical problems in the space [43]. Owing to the advantages of POS, such as ease of use, fast convergence, and good robustness, it is suitable for damage identification in engineering. However, PSO also has some disadvantages, such as prematurity in the search process and ease of falling into the local optimum. There are some experts and scholars to study how to solve the balance between local search and global search [44, 45]. Chen et al. [46] proposed a particle swarm optimization algorithm with crossover operation (PSOCO). By performing crossover on the personal historical best position of each particle, the effective guiding exemplars are constructed, and they maintain a good diversity. In turn, these high-quality exemplars are used to guide the evolution of particles. Through adopting lots of benchmarks with different characteristics in the experiments, it is proved that PSOCO is a competitive PSO variant for some benchmark functions. Tran-Ngoc et al. [47] improved the calculation method of PSO's inertia weight factor by introducing contraction factor K to improve the disadvantage of premature convergence of PSO. Then, the best local position of particles in PSO based on orthogonal diagonalization (OD) was arranged, which greatly reduced the calculation cost of PSO. The Guadalquivir bridge model in Spain is modified by using ODIPSO, which shows that ODIPSO not only improves the effectiveness of the PSO algorithm but also greatly reduces the computational time. Khatir et al. [48] proposed a new technique based on an artificial neural network (ANN) combined with particle swarm optimization (PSO) for damage quantification in laminated composite plates using the Cornwell indicator (CI). Isogeometric analysis (IGA) is used as a modeling technique, CI is used as the input data, and damage locations and severities are used as the output data. The numerical simulation result indicates that high accuracy of damage quantification is achieved using ANN-PSO-IGA-CI. Furthermore, it is demonstrated that substantial savings in computational time are achieved when using ANN-PSO-IGA-CI compared with PSO-IGA-CI. According to the disadvantages of PSO, the calculation method of inertia weight of PSO is improved in this paper, which can balance the relationship between local search and global search of PSO, so as to avoid premature or local optimum in the process of PSO optimization calculation.

A simple, yet powerful, technique based on wavelet transform combined with the improved particle swarm optimization (WIPSO) algorithm for microdamage location and quantification in the structure is proposed, and the microdamage of the structure is defined within 10%. First, the structural strain mode is calculated by using the structural modal data, and the wavelet coefficient diagram is obtained by wavelet transform of the strain mode. According to the singularity of the wavelet coefficient, the structural damage location can be directly determined from the wavelet coefficient diagram. Then, according to the known damage location of the structure, MATLAB is utilized to model the structure and calculate the parameters of the objective function. Finally, MATLAB is applied to run IPSO to calculate the optimal solution of the objective function of the structural damage location in order to calculate the damage severity of the structural damage location. IPSO improves the calculation method of the inertial weight of the standard PSO to balance the global and local searches of damage identification, so the IPSO will not fall into the local optimization and prematurity in research problems similar to those in this paper. Through numerical simulations of a fixed beam structure and a one-story one-span frame structure, the accuracy and running speed of structural damage identification by WIPSO are obtained. Then, IPSO is compared with GA [44, 49], 0.8PSO, and BA [50] to obtain the performance. The numerical simulation and experimental research under different damage scenarios show that WIPSO can quickly and accurately identify the structural damage and has great potential in damage identification of structures.

2. The Principle of Wavelet Singularity

Considering the function $\psi(t) \in L^1(R) \cap L^2(R)$ and $\int_{-\infty}^{+\infty} \psi(t)\mathrm{d}t = 0$, $\psi(t)$ is called a basic wavelet or a mother wavelet. $\psi(t)$ is scaled and translated as

$$\psi_{a,b}(t) = \frac{1}{\sqrt{|a|}}\psi\left(\frac{t-b}{a}\right), a, b \in R, a \neq 0, \tag{1}$$

where a and b are the scale factor and translation factor, respectively, and $\psi_{a,b}(t)$ is the wavelet function.

Defining $\psi(t)$ as the basic wavelet, the continuous wavelet transform (CWT) of $f(t) \in L^2(R)$ is defined as

$$Wf(a,b) = \frac{1}{\sqrt{|a|}}\int_{-\infty}^{+\infty} f(t)\psi^*\left(\frac{t-b}{a}\right)\mathrm{d}t = \langle f, \psi_{a,b}\rangle, \tag{2}$$

where $a \neq 0$, b, t is a continuous variable, and $\psi^*(t)$ is the complex conjugate of $\psi(t)$.

The convolution form of the wavelet transform is

$$Wf(a,b) = \frac{1}{\sqrt{|a|}} \int_{-\infty}^{+\infty} f(t)\psi^*\left(\frac{t-b}{a}\right)\mathrm{d}t = \sqrt{|a|} f * \widehat{\psi}_{|a|}(b), \tag{3}$$

where $\widehat{\psi}_{|a|}(t) = |a|^{-1}\psi^*(-t/a)$.

Defining $\theta(t)$ as a smooth function and derivative, $\psi(t) = \mathrm{d}\theta(t)/\mathrm{d}t$, of any low-pass function $\theta(t)$, is the band-pass function, which satisfies $\int_{-\infty}^{+\infty}\psi(t)\mathrm{d}t = 0$, and the wavelet function with scale factor s is

$$\psi_s(t) = \frac{1}{s}\psi\left(\frac{t}{s}\right) = \frac{1}{s}\frac{\mathrm{d}\theta(t/s)}{\mathrm{d}t} = \frac{\mathrm{d}\theta_s(t)}{\mathrm{d}t}. \tag{4}$$

The continuous wavelet transform of the basic wavelet corresponding to function f on s is

$$Wf(s,u) = s^{(1/2)}\left(f * \bar{\psi}_s\right)(u) = s^{(1/2)}\frac{\mathrm{d}}{\mathrm{d}u}\left(f * \bar{\theta}_s\right)(u), \tag{5}$$

where $s > 0$, and equation (5) shows that the modulus maximum $|Wf(s,u)|$ of the wavelet transform is the maximum of the first derivative of f smoothed by $\bar{\theta}_s$ and corresponds to the singular point of the signal.

3. Damage Location Identification

At the moment of damage, the mass of the beam structure with the microdamage is basically the same, so it can be considered that the structural damage is essentially the reduction of stiffness EI. The stiffness of both sides of the damaged location is not equal, i.e., $EI(v^+) \neq EI(v^-)$. When $v = x$, the deformation condition and internal force balance condition of the position still meet the following conditions [18]:

Vertical displacement:

$$w(v^+) = w(v^-). \tag{6}$$

Rotation angle:

$$\frac{\mathrm{d}w(v^+)}{\mathrm{d}x} = \frac{\mathrm{d}w(v^-)}{\mathrm{d}x}. \tag{7}$$

Bending moment:

$$EI(v^+)\frac{\mathrm{d}^2w(v^+)}{\mathrm{d}x^2} = EI(v^-)\frac{\mathrm{d}^2w(v^-)}{\mathrm{d}x^2}. \tag{8}$$

Shearing force:

$$EI(v^+)\frac{\mathrm{d}^3w(v^+)}{\mathrm{d}x^3} = EI(v^-)\frac{\mathrm{d}^3w(v^-)}{\mathrm{d}x^3}, \tag{9}$$

where the superscripts + and − are used to denote the quantities just at the right and left of the discontinuous point. k is the curvature of the section, $\rho(x)$ is the radius of curvature, M is the bending moment, ε is the strain, μ is the severity of deformation, and h is the distance from the point on the section to the neutral layer.

According to equations 8 and (9), microdamage will also cause the curvature mode and strain mode on both sides of the damage location to be unequal. In addition, the curvature mode and strain mode, far away from the damage location of the structure, will not change greatly, so the curvature mode and strain mode of the structure will mutate at the damage location. Previous research studies show that the strain mode is more sensitive to the microdamage of the structure, so the strain mode of the damaged structure will be analyzed by the continuous wavelet transform in this study, and the singular point (modulus maximum point) of the structural strain mode signal will be used to identify the damage location of the structure.

4. Strain Mode

Strain is the first derivative of displacement, so each displacement mode corresponds to the corresponding strain mode, and the strain mode reflects the inherent characteristics of the structure. To measure strain, the curvature mode can be used for indirect measurement. According to the material mechanics, the bending static relation of the beam can be obtained as

$$\rho_i = \frac{1}{d_i} = \frac{M_i}{E_iI_i}, \tag{10}$$

where i is the section position of measuring point i, M_i is the bending moment of section i, E_iI_i is the flexural rigidity of section i, d_i is the radius of curvature at section i, and ρ_i is the curvature of section i. According to the approximate equation of bending deformation of the beam,

$$\rho = \frac{\mathrm{d}^2y}{\mathrm{d}x^2}, \tag{11}$$

where x is the coordinate along the length direction of the straight beam and y is the bending deflection of the beam. According to equations (10) and (11), the difference equation of three equidistant continuous measuring points along the beam can be obtained:

$$\rho_i = \frac{M_i}{E_iI_i} = \frac{y_{i+1} - 2y_i + y_{i-1}}{\Delta^2}, \tag{12}$$

where $i-1$, i, and $i+1$ are three adjacent continuous measuring points with equal distance along the beam, ρ_i is the curvature of section i, y_i is the bending deflection of section i, y_{i+1} and y_{i-1} are the bending deflections of section $i-1$ and section $i+1$ of the measuring points, respectively, and Δ is the bending deflection of two adjacent measuring points. The strain ε_i of the measuring point i of the beam can be expressed as

$$\varepsilon_i = -\frac{h}{d_i} = -h\frac{y_{i+1} - 2y_i + y_{i-1}}{\Delta^2} = -h\rho_i, \tag{13}$$

where h is the distance between the surface of the measuring point on the beam and the neutral layer, and equation (13) shows the direct relationship between the curvature mode and the strain mode of the beam.

5. Improved Particle Swarm Optimization Algorithm

5.1. The Principle of the Standard Particle Swarm Optimization (PSO) Algorithm. The advantages of PSO are that it is simple

to use, converges quickly, and so on. When PSO is used to solve the optimization problem, finite possible solutions of the optimization problem can be initialized to the particle swarm, and the individual fitness and average fitness of the whole population will be continuously improved by an iterative process. After the individual fitness of the particles in the group no longer change significantly or the optimal particle position in the solution space is found, the whole group will stop the iteration, and the optimal position or optimal solution of the optimization problem in the current whole group will be output.

The particle swarm is defined to find the optimal solution in an M-dimensional solution space, and the swarm is initialized with N random particles, the position X_i of the i particle is $X_i = (x_{i_1}, x_{i_2}, \ldots, x_{i_M})$, the velocity is $V_i = (v_{i_1}, v_{i_2}, \ldots, v_{i_M}), i = 1, 2, \ldots, N$, and x and v are the components of X and V in different dimensions, respectively. In the iterative optimization process, the particles will evaluate the current position by the established fitness function $f(x)$, and the individual optimal position $p_{\text{best}} = (p_{i_1}, p_{i_{12}}, \ldots, p_{iM})$ of each particle in the current group and the global extreme value of the whole group are evaluated according to equations (14) and (15):

$$p_{\text{best}}(k+1) = \begin{cases} p_{\text{best}_i}(k), & f\left[X_i(k+1)\right] \geq f\left[p_{\text{best}_i}(k)\right], \\ X_i(k+1), & f\left[X_i(k+1)\right] < f\left[p_{\text{best}_i}(k)\right], \end{cases} \tag{14}$$

$$g_{\text{best}}(k) = \min\left\{f\left[p_{\text{best}_1}(k)\right], f\left[p_{\text{best}_2}(k)\right], \ldots, f\left[p_{\text{best}_N}(k)\right]\right\}, \tag{15}$$

$$v_{im}^{k+1} = wv_{im}^{k} + c_1 r_1\left(p_{im}^{k} - x_{im}^{k}\right) + c_2 r_2\left(g_{im}^{k} - x_{im}^{k}\right), \tag{16}$$

$$x_{im}^{k+1} = x_{im}^{k} + v_{im}^{k}, \tag{17}$$

where k is the number of current iteration steps, $i = 1, 2, \ldots, N$, $m = 1, 2, \ldots, M$, and w is the inertia weight factor, which controls the search range. When w is large, PSO focuses on global search, while when w is small, PSO focuses on local search. c_1 and c_2 are nonnegative acceleration factors (or learning factors) that control the self-learning ability and social learning ability of particles, respectively; r_1 and r_2 are the random values in $[0, 1]$. Individual extremum p_{best} and global extremum g_{best} are tracked by equations (14) and (15), respectively, and the velocity V and position X of particles in the group are updated iteratively by equations (16) and (17), so the algorithm starts the next iteration cycle. PSO terminates the iteration and outputs the optimal particle position in the current group when the particle obtains the optimal solution of the fitness function or the algorithm meets the iteration stop condition.

5.2. Improved Particle Swarm Optimization (IPSO) Algorithm. Although PSO has advantages in solving complex optimization and combination problems, there are many disadvantages of PSO, such as its poor local search ability, low search accuracy, and ease of falling into the local minimum. These problems are all due to the dependence of PSO on parameters and the imperfection of the algorithm theory. PSO improvement can be summed up with the following two aspects: (1) improve the theory of PSO and improve the parameters on which it depends to overcome its own shortcomings; (2) introduce other excellent theories and algorithms, through the combination with PSO, to overcome the shortcomings of PSO.

In this paper, we improve the parameters of PSO by the first approach to overcome the problem that PSO has easy precocity and falls into the local optimum. In PSO, choosing the right parameters to optimize the performance of the algorithm is a complex problem. The main control parameters of PSO include population size N, inertia weight factor w, acceleration factors c_1, c_2, maximum speed, stopping criterion, neighborhood structure setting, and boundary condition processing strategy. The number of population size number N in these parameters affects the convergence speed of the algorithm and whether the algorithm easily falls into the local optimum. The value of N is set smaller, and the convergence speed of the algorithm is faster; however, it easily falls into the local optimum. When the value of N is set larger, the PSO optimization ability is good, and the convergence speed of the algorithm is slow. When the number of particles increases to a certain level, the increase no longer has a significant effect. Therefore, according to the setting of specific problems, the value of N generally ranges from 10 to 50. For more complex problems, the value of N can be 100 or more. Learning factors c_1, c_2 have the ability to self-summarize and learn from the excellent individuals in the group, which regulates the maximum step length of particles flying in the individual optimal direction and the group optimal direction, respectively. When the learning factor is small, particles may wander far from the target area, while when the learning factor is large, particles move quickly to the target area or even cross the target. Therefore, in order to balance the individual experience and group experience of particles, c_1, c_2 can generally be taken as 2. In equation (16), the inertia weight w indicates to what extent the original speed is retained. If w is larger, the global search ability is stronger, and if w is smaller, the local search ability is stronger. According to different calculation methods of inertia weight, different functional PSOs can be devolved.

In this paper, the calculation method of inertia weight factor w in equation (16) is improved to enhance the convergence performance of PSO; however, the value of w is not a fixed value or a linearly increasing and decreasing value to achieve the purpose of optimizing PSO. Thus, the dynamic adjustment method is considered. PSO will converge faster in the early stage while calculating. To maintain a certain level of particle search speed, according to the relationship between the maximum number of iterations and the current number of iterations, as well as the output value of the current objective function and the average value of all the current

calculated objective functions, a calculation method of w can be established to achieve the purpose of PSO. The calculation method of w for IPSO is as follows:

$$w = \begin{cases} w_{\max} - \dfrac{t \times (w_{\max} - w_{\min})}{T}, & F \le F_{\text{avg}}, \\ w_{\max}, & F > F_{\text{avg}}, \end{cases} \tag{18}$$

where $w_{\max}$ and $w_{\min}$ are the maximum and minimum values of inertia weight, with values of 0.9 and 0.4, respectively. T is the maximum number of iterations, and t is the current number of iterations. F is the current objective function value, and F_{avg} is the average objective function value of all particles. When the target value of each particle tends to be the same or local optimum, the inertia weight increases, and when the target value of each particle is relatively scattered, the inertia weight decreases.

The steps required for IPSO to identify the severity of the structural damage are as follows:

5.2.1. Establishing the Unknown Function. The method of element stiffness reduction is used to simulate the damage severity γ_i of the structural damage element, and the unknown value γ of the objective function is constructed by taking γ_i of all structural damage elements to be identified as an unknown component. In this paper, the method of reducing the element stiffness is used to simulate the damage. If the stiffness of the damaged element is EI, the damage severity is γ, and the stiffness of the damaged element is EI_i:

$$EI_i = (1 - \gamma)EI. \tag{19}$$

Since the damage is set as a minor damage, it is assumed that the mass and modulus of elasticity E of the damaged element do not change before and after damage, but the moment of inertia of the element changes. According to the method of setting the element damage, the height of the element changes before and after damage in this paper.

5.2.2. Constructing the Objective Function. Based on the comprehensive consideration of the global and local structural properties, the objective function shown in equation (20) is constructed by using the regularized frequency variation function and the weighted sum of the displacement mode variation function:

$$\min F = F_\omega \sum_{i=1}^{m} \left(\frac{f_i^{\text{test}} - f_i^{\text{cal}}(\gamma)}{f_i^{\text{test}}} \right)^2 + F_\phi \sum_{i=1}^{n} \sum_{j=1}^{k} \left(\phi_{ij}^{\text{test}} - \phi_{ij}^{\text{cal}}(\gamma) \right)^2, \tag{20}$$

where F_ω and F_ϕ are weighting factors, which are set as 1, f_i^{test} and f_i^{cal} are the measured and calculated i-th order natural frequencies, respectively, ϕ_{ij}^{test} and ϕ_{ij}^{cal} are the measured and calculated displacement modes of the i-th order j-th node, respectively, after normalization, m is the order of the natural frequency, n is the order of the displacement mode, and k is the node number. The unknown value γ of the minimum value of the objective function $\min F$ is the set of damage severity γ_i of all damage elements of the structure.

5.2.3. Establishing the Fitness Function. In this study, $\min F$ is taken as the fitness function $FIT1$ of IPSO to identify the damage severity of the structure, i.e., $FIT1 = \min F$. The particles of the group also search for the optimal solution in the solution space based on the minimum value of $\min F$.

5.2.4. Establishing IPSO and Solving the Fitness Function. Before solving $\min F$ with IPSO, the relevant parameters of the algorithm are set. The value of particle n ranges from 0 to 0.9, and the number of particles N ranges from 50 to 100; w is calculated with equation (18), the values of c_1 and c_2 are set as 2, the value of the maximum number of iterations T ranges from 100, and the value of accuracy error e for the optimal solution is set as 0.0001.

After setting the relevant parameters, it is necessary to adjust the mode parameters of the model according to the test data, so as to eliminate the modeling errors as much as possible. Then, the IPSO code is debugged according to the optimization problem to determine the parameter settings to complete identification of the structural damage.

The flowchart of structural damage identification by combining the wavelet transform with IPSO is shown in Figure 1, which shows the combination of the wavelet and the intelligent algorithm to identify the structural damage.

6. Numerical Simulation

To verify the ability of WIPSO proposed in this study, a wavelet analysis and four kinds of intelligent algorithms are used to identify the location and severity of the structural damage under two damage scenarios. Scenario 1 uses a fixed beam as the object. Scenario 2 uses a one-story one-span frame structure as the object.

6.1. Scenario 1. A fixed beam model is shown in Figure 2. The fixed beam span is 1118 mm, the section size is $b \times h = 60\,\text{mm} \times 80\,\text{mm}$, Q235 steel is used, the material density is $\rho = 7800\,\text{kg/m}^3$, Poisson's ratio is $\mu = 0.3$, and the elastic modulus is $E = 2.1 \times 10^{11}\,\text{N/m}^2$. According to structural parameters, ANSYS finite element software is used to model the fixed beam. Point A and point B of the beam end adopt the form of fixed support, so the beam end has no displacement in any direction, as shown in Figure 2. The finite element model of the fixed beam is divided into 43 elements in the order of $A - B$, as shown in Figure 2, and the element nodes are coded in turn. The damaged elements and damage severity of the fixed beam are set as follows: the damage severity of element 12 is 4%, the damage severity of element 25 is 20%, and the damage severity of element 38 is 10%. The method of reducing the element stiffness is

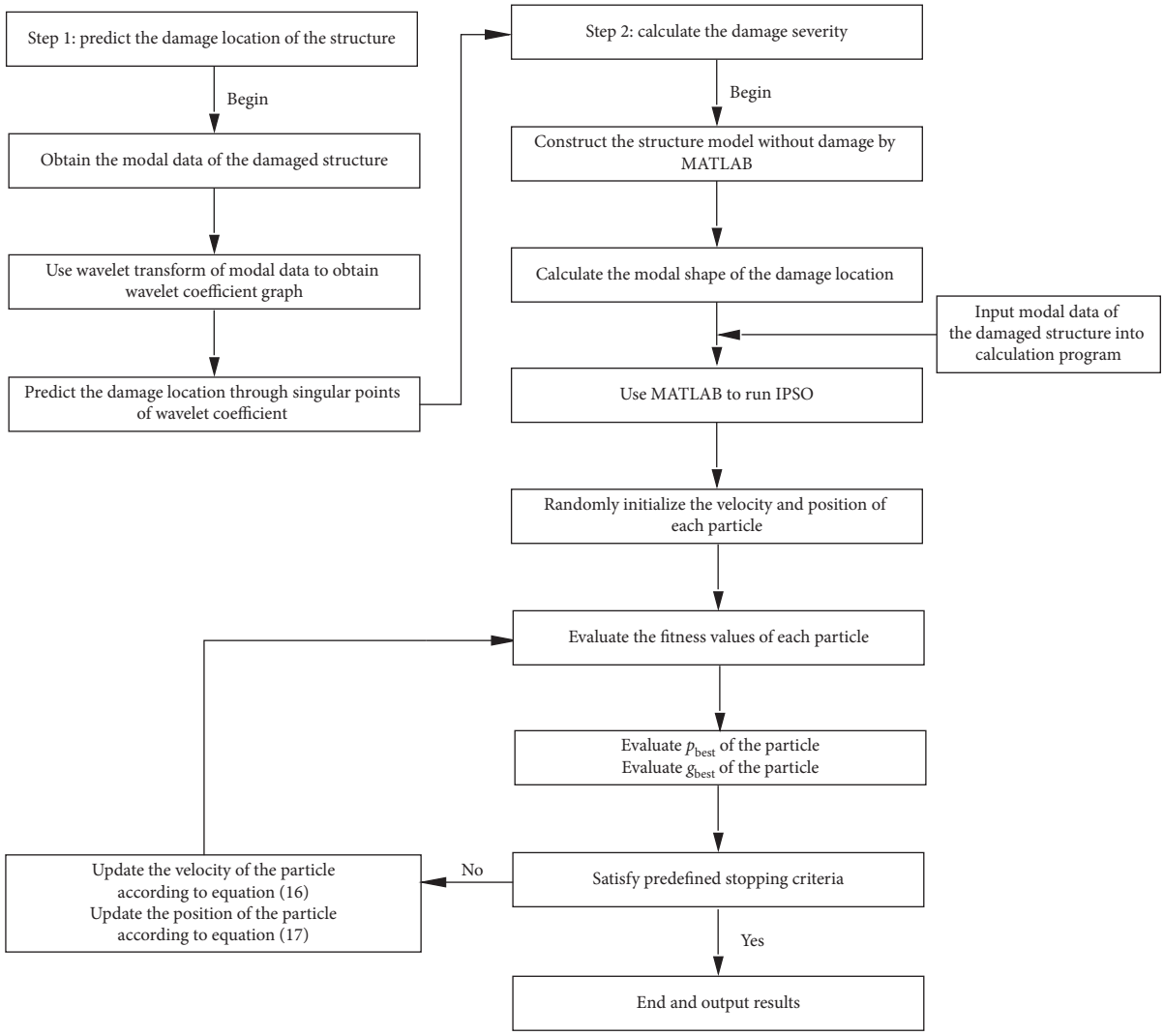

Figure 1: Damage identification flowchart of WIPSO.

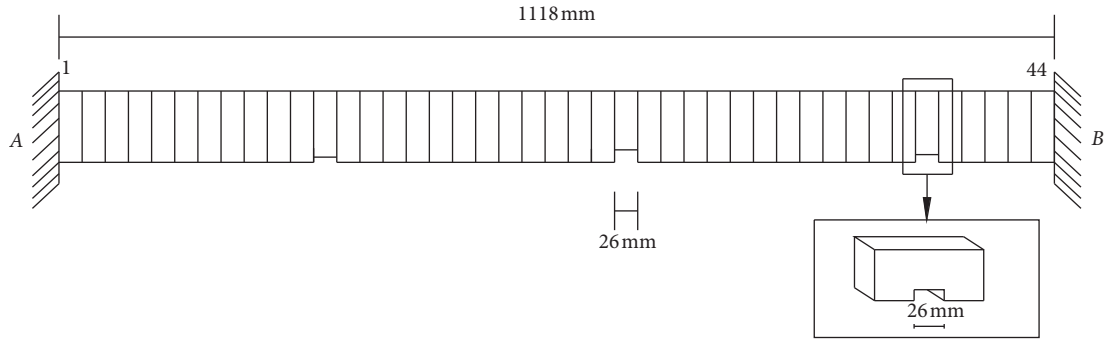

Figure 2: The fixed beam with damages.

adopted in the damage simulation, and the damage form is transfixion notch along the thickness direction. By comparing the accuracy and running time of the structural damage identified by four intelligent algorithms, the calculation speed, accuracy, and stability of IPSO can be obtained.

6.2. Identification of the Damage Location. The finite element model of the fixed beam structure is established by ANSYS finite element software. According to scenario 1, elements 12, 25, and 38 are set as damage elements, and the displacement mode of the structure is calculated by ANSYS. According to the calculation method of the strain mode

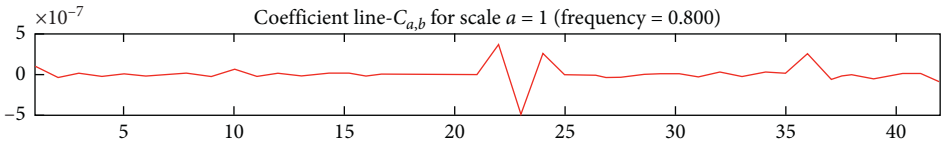

Figure 3: Wavelet coefficients.

described in Section 4, the second-order derivation of the displacement mode is carried out by MATLAB to obtain the strain mode of the structure. Then, the wavelet toolbox in MATLAB is used to select the DB wavelet to transform the strain modal data, and the wavelet coefficient shown in Figure 3 can be obtained.

It can be seen from Figure 3 that the wavelet coefficient diagram of the fixed beam structure suddenly changes near points 10, 23, and 36. The strain mode data calculated by the second-order derivation of the displacement mode with MATLAB will be reduced by two. Therefore, points 10, 23, and 36 in the wavelet coefficient diagram actually correspond to elements 12, 25, and 38 in the fixed beam structure model. There will be mutations around the damage location that are affected by the damage, but the maximum value point of the modulus corresponds to the damage location. According to the above statement, fixed beam structure damage occurs in elements 12, 25, and 38, which is consistent with the damage element setting of the finite element model of the fixed beam. Therefore, the wavelet singularity principle can accurately identify the structural damage location.

6.3. Identification of Damage Severity. According to Figure 2, the fixed beam is modeled with MATLAB, and the beam structure is divided into 43 elements according to the order of $A - B$. Point A is taken as point 1 and point B is taken as point 44 to number the element nodes in turn. According to the number sequence, the element stiffness is assembled to obtain the overall stiffness, thus completing the modeling. The codes of IPSO, 0.8PSO, GA, and BA are compiled by MATLAB, respectively. Since the damage location has been identified, only the damage severity of the damage element needs to be taken as the unknown value of the fitness function. MATLAB is utilized to calculate the natural frequency and displacement mode shape of the model according to the beam model, which is substituted into the fitness function to calculate the damage severity, as shown in the calculation flowchart in Figure 1. To reduce the randomness of the algorithm, the four intelligent algorithms will run on the same computer ten times. Because of the randomness of the calculated results in each operation, the maximum and minimum values will not be removed from the calculated results to ensure the fairness of each calculated result.

(1) The structural damage severity graph and calculation error graph, calculated by 0.8PSO, are shown in Figures 4 and 5, respectively.

Figures 4 and 5 show that the accuracy of 0.8PSO in identifying the structural damage severity is relatively low, and its maximum error reaches 1%. This indicates that the particle swarm optimization algorithm with fixed inertia weight factor may fall into premature or local optimal solution, which caused high identification error.

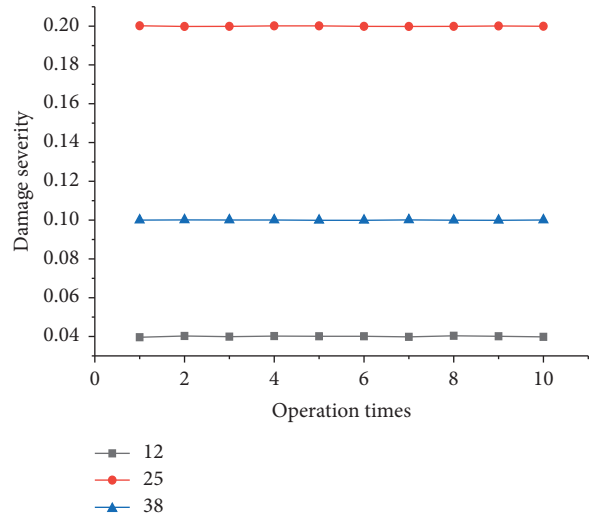

Figure 4: Damage severity identification of 0.8PSO.

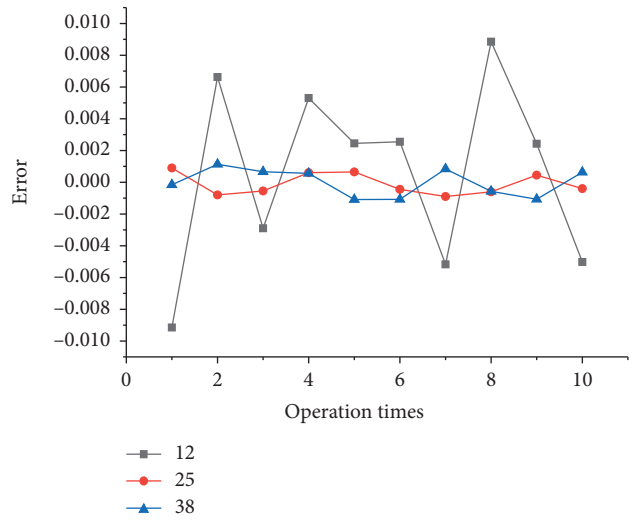

Figure 5: Error of 0.8PSO.

(2) The structural damage severity graph and calculation error graph, calculated by GA, are shown in Figures 6 and 7, respectively.

The accuracy of GA in identifying the structural damage severity is high, and the evaluation errors are within 0.5%, as shown in Figures 6 and 7. The higher

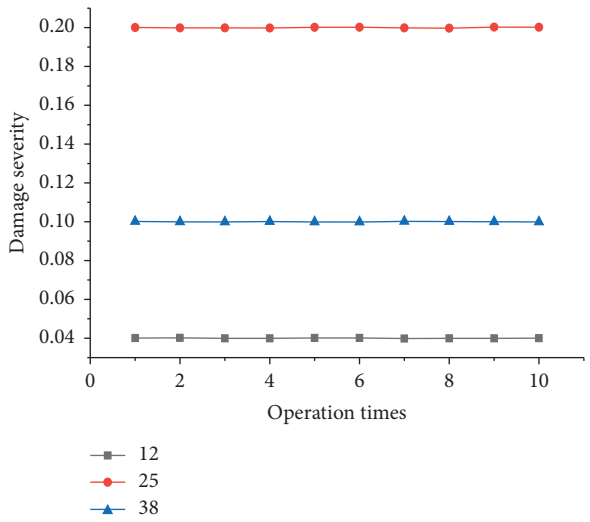

Figure 6: Damage severity identification of GA.

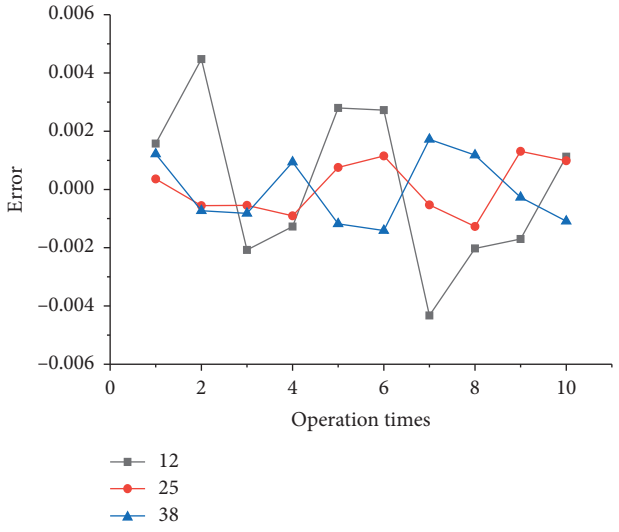

Figure 7: Error of GA.

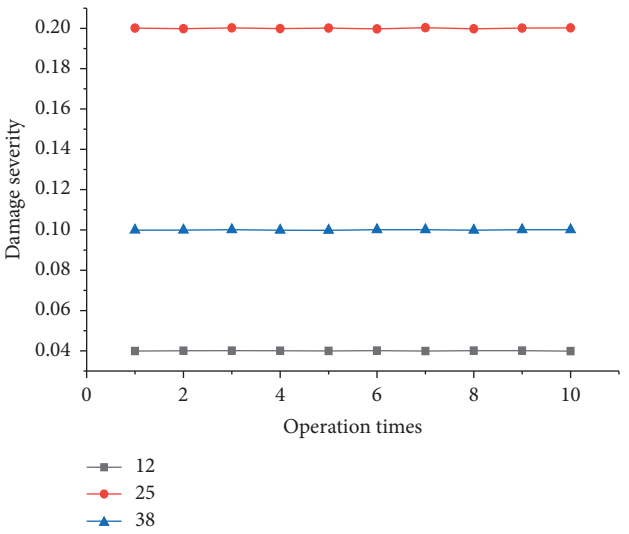

Figure 8: Damage severity identification of BA.

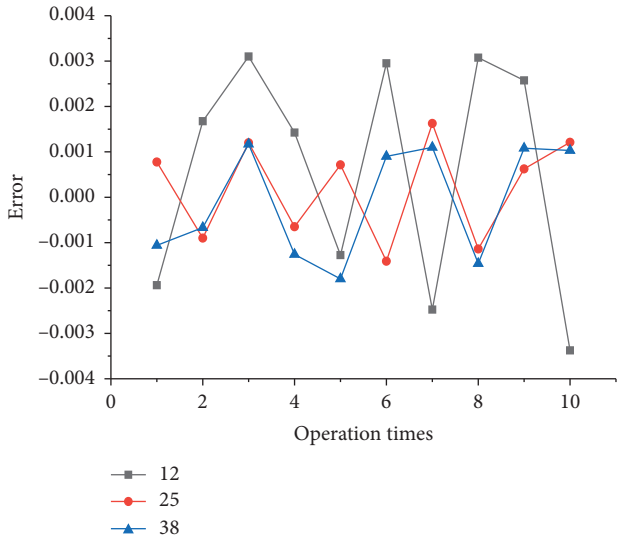

Figure 9: Error of BA.

the damage severity is, the smaller the damage error fluctuation is.

(3) The structural damage severity graph and calculation error graph, calculated by BA, are shown in Figures 8 and 9, respectively.

The accuracy of BA in identifying the structural damage severity is high, and its error is within 0.4%, as shown in Figures 8 and 9. The higher the damage severity is, the smaller the damage error is.

(4) The structural damage severity graph and calculation error graph, calculated by IPSO, are shown in Figures 10 and 11, respectively, and it can be found that the accuracy of IPSO in identifying the damage severity of the structure is very high, and the evaluation errors are within 0.25%. The higher the damage severity is, the smaller the damage error fluctuation is.

Figure 12 shows the running time ratio of GA, BA, 0.8PSO, and IPSO to IPSO′, and IPSO′ is the average of the running time of IPSO. Figure 12 shows that GA takes the longest time to identify beams with three damage areas, while BA takes the shortest time, and IPSO takes slightly more time than BA.

Figures 13(a) and 13(b) illustrate the curves of the objective functions and iteration times obtained by randomly selecting 0.8PSO and IPSO to run for ten times. Table 1 shows the iterations and objective function values of 0.8PSO and IPSO running for ten times. It can be seen from Figure 13 and Table 1 that although the iteration curve of 0.8PSO is similar to that of IPSO, the number of iterations of 0.8PSO in each operation reaches $T_{\max} = 100$, while that of IPSO in each operation is $T < 100$. The objective function value $\min F$ calculated by 0.8PSO is much larger than that calculated by IPSO. The above analysis indicates that IPSO is effective for the improvement of inertia weight, and there is

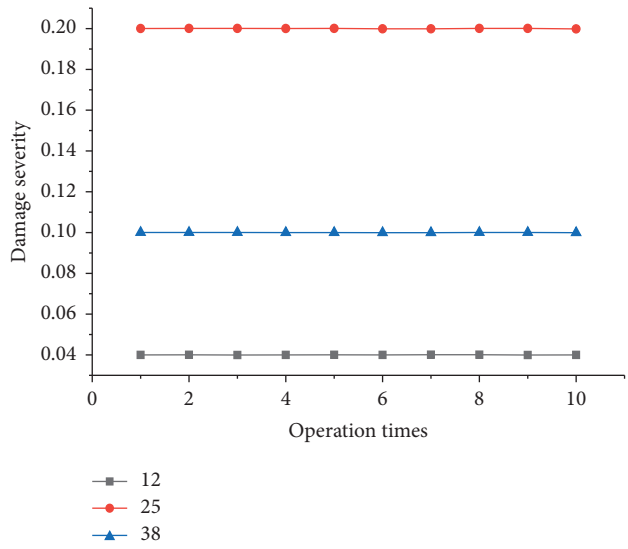

Figure 10: Damage severity identification of IPSO.

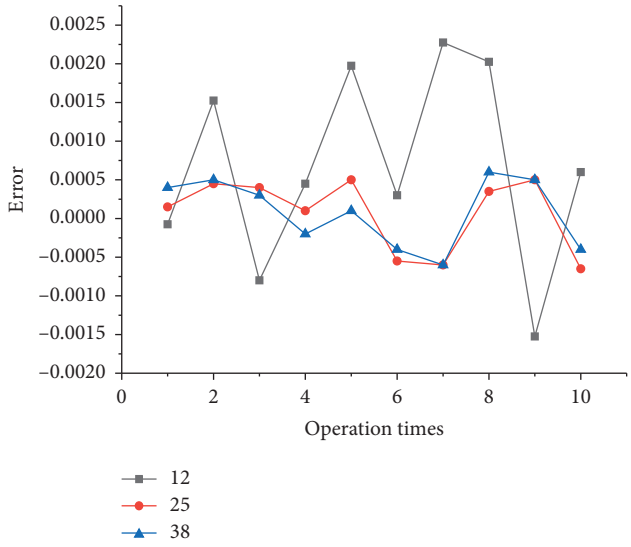

Figure 11: Error of IPSO.

no premature or local optimization of IPSO in the identification problem.

It can be seen from the above analysis that although IPSO takes 1/3 more time to identify the structural damage than BA, its identification accuracy is higher than BA, and the error fluctuation of IPSO in identifying the structural damage is the smallest with 0.25%.

6.4. Scenario 2. A one-story one-span frame structure is depicted in Figure 14. A rigid connection is adopted between the beams and columns of the frame structure, and the connection between the columns and the ground is a fixed connection. The beam span and column height are 4500 mm, the section size is $b \times h = 300\,\text{mm} \times 500\,\text{mm}$, Q235 steel is used, the material density is $\rho = 7800\,\text{kg/m}^3$, Poisson's ratio is $\mu = 0.3$, and the elastic modulus is $E = 2.1 \times 10^{11}\,\text{N/m}^2$. According to the above parameters, ANSYS finite element

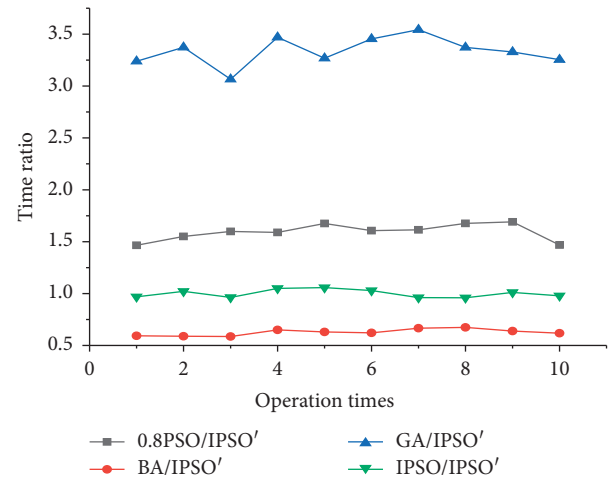

Figure 12: Ratios of running time of the four algorithms.

software is used to model the one-story one-span frame structure. Point A and point D of the frame structure adopt the form of fixed support so that the frame structure end has no displacement in any direction, as shown in Figure 14. The finite element model of the frame structure is divided into 450 elements in the order of $A - B - C - D$, as shown in Figure 14, and the element nodes are coded in turn. The damaged elements and damage severity of the frame structure are set as follows: the damage severity of element 116 is 9%, the damage severity of element 203 is 3%, and the damage severity of element 391 is 7%. The method of reducing the element stiffness is adopted in the damage simulation, and the damage form is transfixion notch along the thickness direction. By comparing the accuracy and running time of the structural damage identified by four intelligent algorithms, the calculation speed, accuracy, and stability of IPSO can be obtained.

6.5. Identification of the Damage Location. The finite element model of the one-story one-span frame structure is established by ANSYS finite element software. According to scenario 2, elements 116, 203, and 391 are set as damage elements, and the displacement mode of the structure is calculated by ANSYS. According to the calculation method of the strain mode described in Section 4, the second-order derivation of the displacement mode is carried out by MATLAB to obtain the strain mode of the structure. Then, the wavelet toolbox in MATLAB is used to select the DB wavelet to transform the strain modal data, and the wavelet coefficient shown in Figure 15 can be obtained.

It can be seen from Figure 15 that the wavelet coefficient diagram of the one-story one-span frame structure suddenly changes near points 114, 201, and 389. The data of the strain mode calculated by the second-order derivation of the displacement mode with MATLAB will be reduced by two. Therefore, points 114, 201, and 389 in the wavelet coefficient diagram actually correspond to elements 116, 203, and 391 in the frame structure model. There will be mutations around the damage location that are affected by the damage, but the

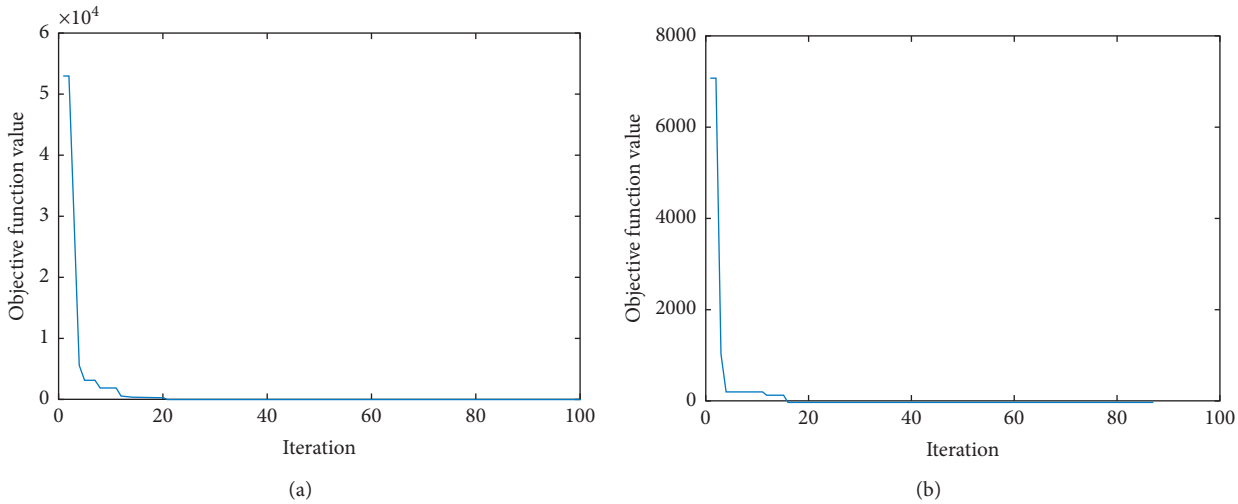

Figure 13: The relationship between the objective function and the iterations. (a) 0.8PSO. (b) IPSO.

Table 1: Iterations and objective function values of 0.8PSO and IPSO, respectively.

Times	0.8PSO		IPSO	
	Iterations	min F	Iterations	min F
1	100	0.10244	74	$5.32E-05$
2	100	0.073985	75	$9.87E-05$
3	100	0.26458	85	$6.07E-05$
4	100	0.097732	85	$9.15E-05$
5	100	0.039742	88	$9.89E-05$
6	100	0.175657	88	$5.77E-05$
7	100	0.033481	88	$9.76E-05$
8	100	0.035378	88	$8.63E-05$
9	100	0.01116	88	$7.73E-05$
10	100	0.00252	88	$8.69E-05$
Average value	100	0.072668	84.7	$8.09E-05$

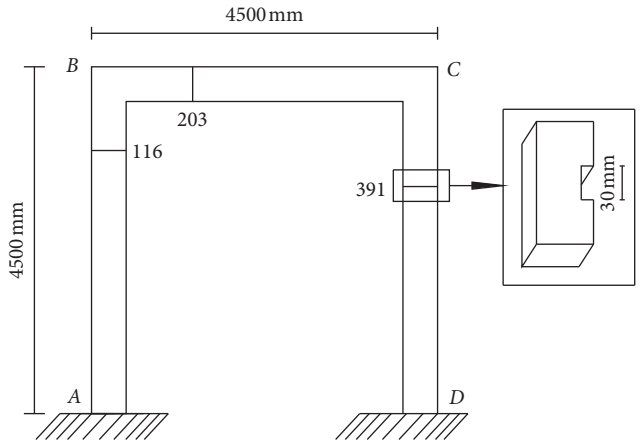

Figure 14: Frame structure with damages.

maximum value point of the modulus corresponds to the damage location. According to the above statement, frame structure damage occurs in elements 116, 203, and 391, which is consistent with the damage element setting of the finite element model of the one-story one-span frame structure. Therefore, the wavelet singularity principle can accurately identify the structural damage location.

6.6. Identification of Damage Severity. According to Figure 14, the one-story one-span frame structure is modeled with MATLAB, and the frame structure is divided into 450 elements according to the order of $A-B-C-D$. Point A is taken as point 1 and point D is taken as point 451 to number the element nodes in turn. According to the number sequence, the element stiffness is assembled to obtain the overall stiffness, thus completing the modeling. The codes of IPSO, 0.8PSO, GA, and BA are compiled by MATLAB, respectively. Since the damage location has been identified, only the damage severity of the damage element needs to be taken as the unknown value of the objective function. MATLAB is utilized to calculate the natural frequency and displacement mode shape of the model according to the frame structure model, which is substituted into the fitness function to calculate the damage severity, as shown in the calculation flowchart in Figure 1. To reduce the randomness of the algorithm, the four intelligent algorithms will run on the same computer ten times. Because of the randomness of the calculated results in each operation, the maximum and minimum values will not be removed from the calculated results to ensure the fairness of each calculated result.

(1) The structural damage severity graph and calculation error graph, calculated by 0.8PSO, are shown in Figures 16 and 17, respectively.

Figures 16 and 17 show that the maximum error of 0.8PSO in identifying the structural damage severity is 0.6%, and the identification accuracy is slightly higher than that of the fixed beam; however, the error is still high.

(2) The structural damage severity graph and calculation error graph, calculated by GA, are shown in Figures 18 and 19, respectively.

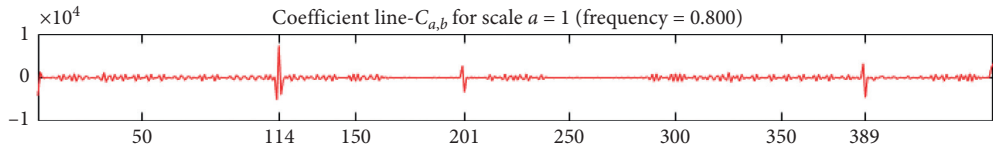

Figure 15: Wavelet coefficients of the frame structure.

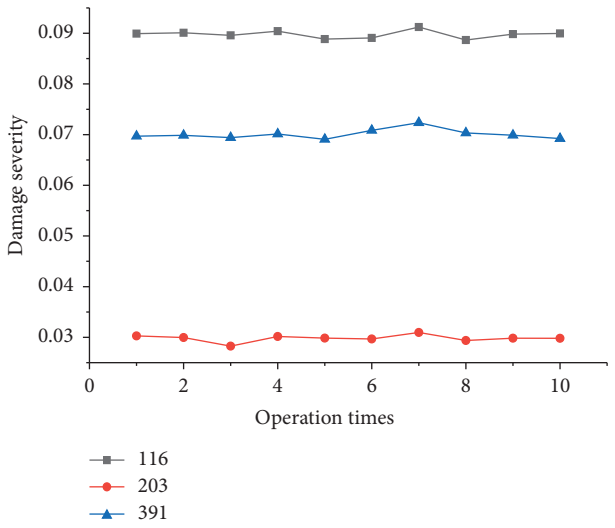

Figure 16: Damage severity identification of 0.8PSO.

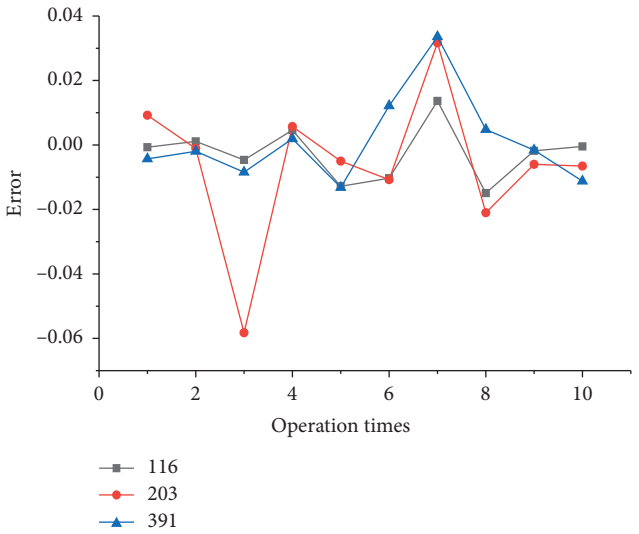

Figure 17: Error of 0.8PSO.

The accuracy of GA in identifying the structural damage severity is high, and the evaluation errors are within 0.3%, as shown in Figures 18 and 19. The higher the damage severity is, the smaller the damage error fluctuation is.

(3) The structural damage severity graph and calculation error graph, calculated by BA, are shown in Figures 20 and 21, respectively.

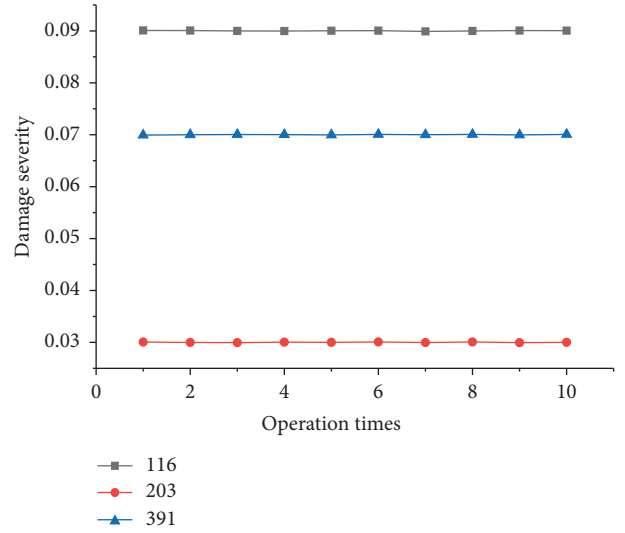

Figure 18: Damage severity identification of GA.

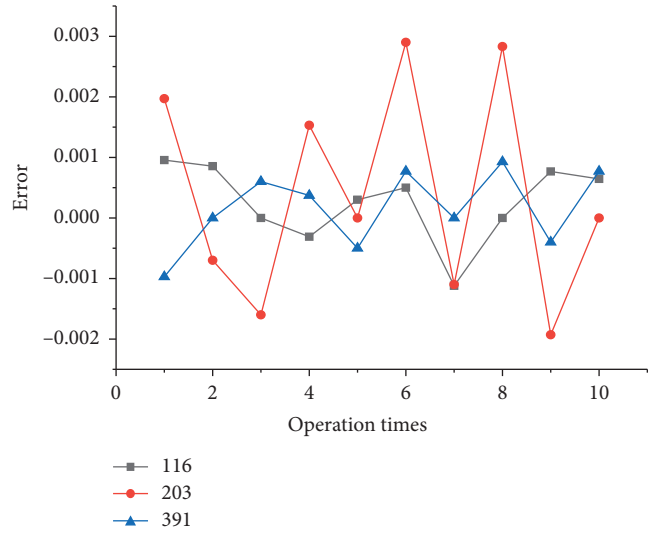

Figure 19: Error of GA.

The accuracy of BA in identifying the structural damage severity is high, and its error is within 0.35%, as shown in Figures 20 and 21. The higher the damage severity is, the smaller the damage error is.

(4) The structural damage severity graph and calculation error graph, calculated by IPSO, are shown in Figures 22 and 23, respectively.

The accuracy of IPSO in identifying the structural damage severity is high, and its error is within 0.3%, as

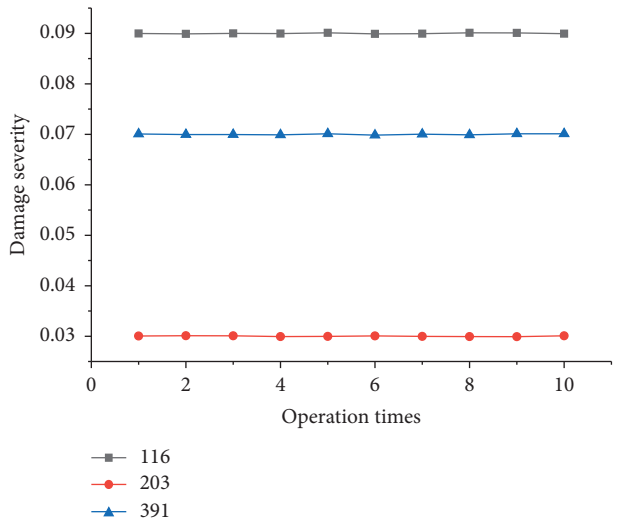

Figure 20: Damage severity identification of BA.

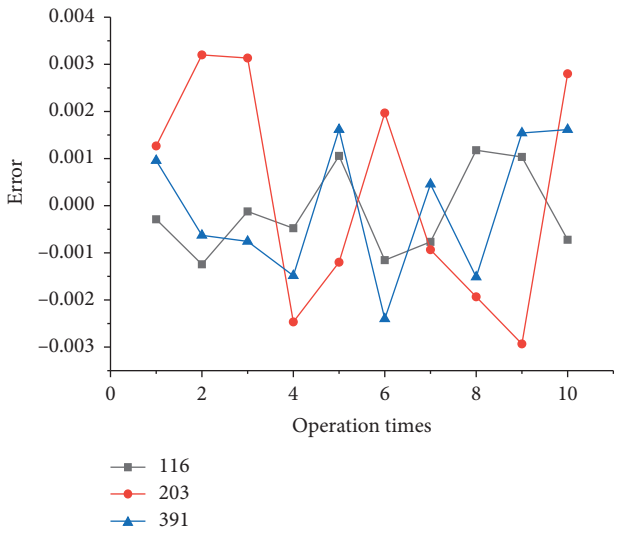

Figure 21: Error of BA.

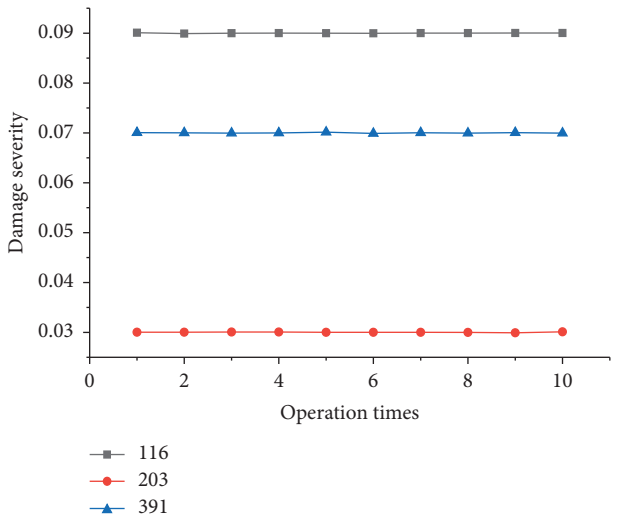

Figure 22: Damage severity identification of IPSO.

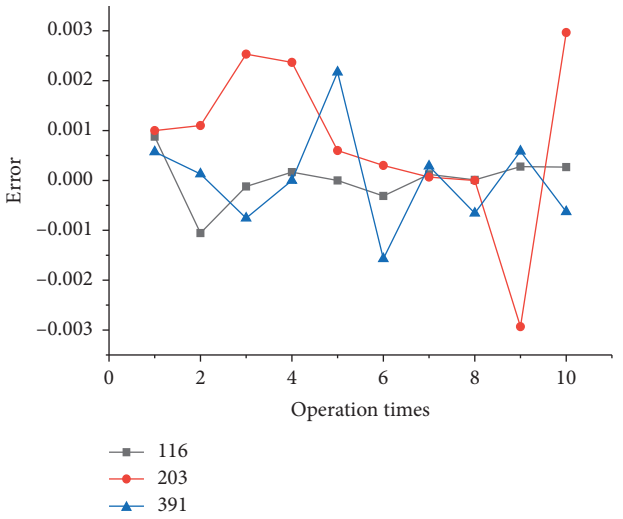

Figure 23: Error of IPSO.

shown in Figures 22 and 23, respectively. The higher the damage severity is, the smaller the damage error is.

The running time ratios of GA, BA, 0.8PSO, and IPSO to IPSO′ are shown in Figure 24, and IPSO′ is the average of the running time of IPSO. Figure 24 shows that GA takes the longest time to identify the frame structure with three damage areas, while BA takes the shortest time, and IPSO takes slightly more time than BA.

Figures 25(a) and 25(b) illustrate the curves of the objective functions and iteration times obtained by randomly selecting 0.8PSO and IPSO to run for ten times. Table 2 shows the iterations and objective function values of 0.8PSO and IPSO running for ten times. It can be seen from Figure 25 and Table 2 that although the iteration curve of 0.8PSO is similar to that of IPSO, the number of iterations of 0.8PSO in each operation reaches $T_{max} = 100$, while that of IPSO in each operation is $T < 100$. The objective function value min F calculated by 0.8PSO is much larger than that

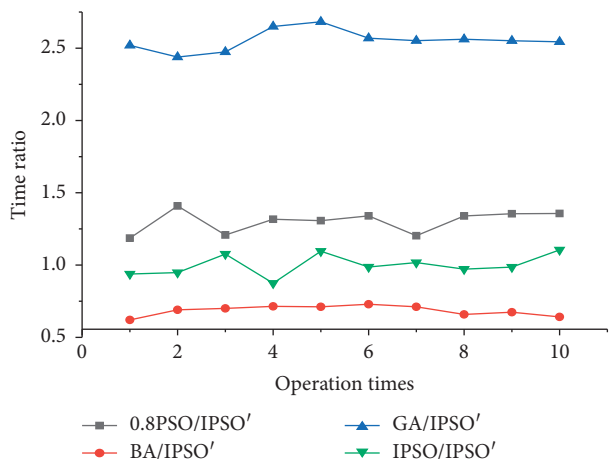

Figure 24: Ratios of running time of the four algorithms.

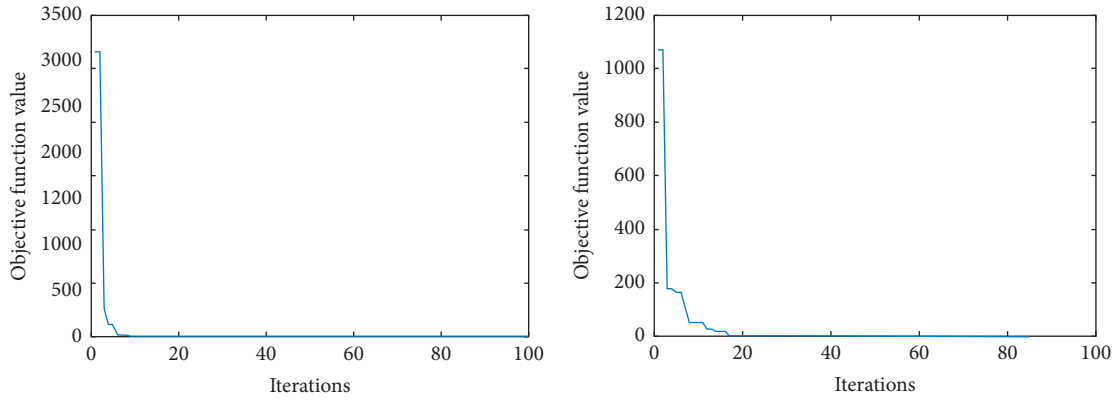

Figure 25: The relationship between the value of the objective function and the iterations. (a) 0.8PSO. (b) IPSO.

Table 2: Iterations and objective function values of 0.8PSO and IPSO, respectively.

Times	0.8PSO		IPSO	
	Iterations	min F	Iterations	min F
1	100	0.030888	67	$4.22E-05$
2	100	0.13869	77	$6.51E-05$
3	100	0.088341	69	$5.78E-05$
4	100	0.097732	69	$8.98E-05$
5	100	0.086453	72	$7.45E-05$
6	100	0.13657	83	$9.56E-05$
7	100	0.059613	86	$9.21E-05$
8	100	0.074612	86	$7.58E-05$
9	100	0.10223	86	$9.45E-05$
10	100	0.085633	85	$9.32E-05$
Average value	100	0.090076	78	$7.81E-05$

calculated by IPSO. The above analysis indicates that IPSO is effective for the improvement of inertia weight, and there is no premature or local optimization of IPSO in the identification problem.

It can be seen from the above analysis that although IPSO takes slightly more time to identify the structural damage than BA, its identification accuracy is higher than BA, and the error fluctuation of IPSO in identifying the structural damage is the smallest and is the same as that of GA.

In conclusion, in the stage of structural damage location identification, singular points of wavelet coefficients can effectively show the structural damage location. In the stage of structural damage severity identification, IPSO takes much less time to identify the damage than GA and slightly more than BA. However, IPSO has the highest damage identification accuracy and the least error fluctuation. This result shows that IPSO can effectively identify structural damage severity and that the accuracy and time of damage identification can reach the level of the current mainstream algorithms. The convergence and damage identification accuracy of IPSO are much better than 0.8PSO, which shows that the improvement of IPSO is effective. Therefore, in the theoretical study, WIPSO can accurately and efficiently identify the structural damage, and IPSO will not premature and fall into the local optimum in damage severity identification of the fixed beam and the frame structure with three damage areas.

6.7. Verification of Noise Effect on the Proposed Method. The influence of noise in recorded signals is unavoidable in real life. Therefore, to investigate the effect of noise on the proposed method, white Gaussian noise is added to the numerical simulation signal to simulate the influence of noise in the experimental situation. In this study, the effect of different noise levels on damage location identification is investigated by applying SNRs 2 and 10 dB.

Using scenario 1 of the numerical simulation as the object, Figure 26 illustrates the wavelet coefficient of three damage areas of the fixed beam without noise. Figures 27(a) and 27(b) show the wavelet coefficient graph with SNRs 2 and 10 dB, respectively. Figures 27(a) and 27(b) show that noise has certain interference on the wavelet coefficient, but the damage location can be easily determined relative to the noise. Figures 27(c) and 27(d) show that the damage location can be easily identified after a certain severity of white noise denoising. Therefore, the method can identify the damage location when a certain severity of noise interference occurs.

7. Experimental Verification

To verify the effectiveness of the proposed method, an experimental study on the beam with fixed support was conducted, as shown in Figure 28. The transfixion damage along the thickness is shown in Figure 29, which is manufactured by a milling machine. A vibration experiment is carried out on a steel beam with a span length of 1300 mm, section size of $b \times h = 60\,\text{mm} \times 80\,\text{mm}$, material density of $\rho = 7800\,\text{kg/m}^3$, Poisson's ratio of $\mu = 0.3$, and elastic modulus of $E = 2.1 \times 10^{11}\,\text{N/m}^2$. The effective experimental length and detailed scenario of the beam are shown in Table 3, and stiffness reduction is used to simulate the damage severity. In the experiment, the beam is excited by percussion with a hammer, and the striking position is 20mm–40 mm near the beam end. The experimental device and sensor layout are shown in Figure 28.

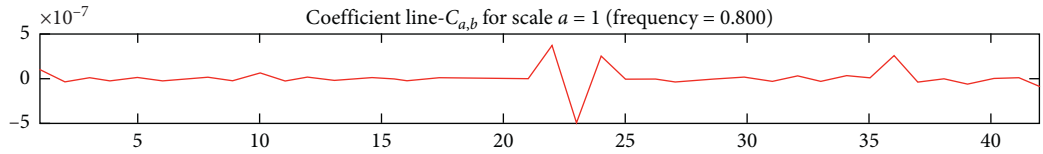

Figure 26: Wavelet coefficients without noise.

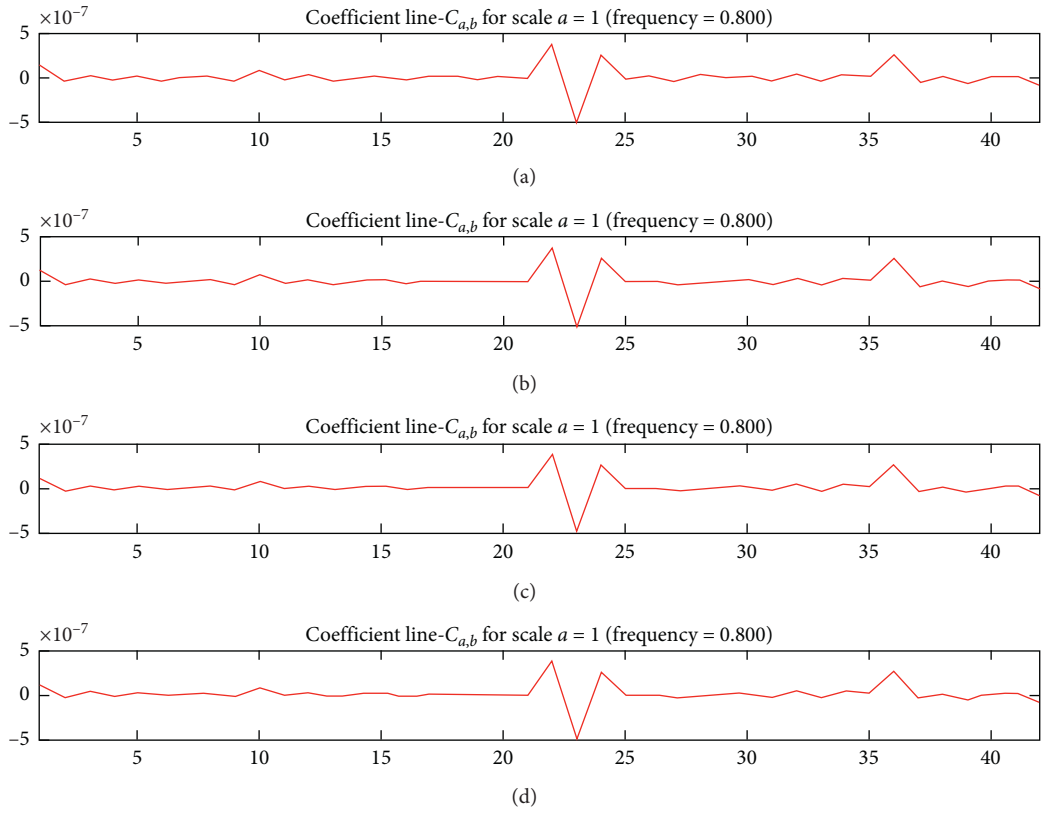

Figure 27: Wavelet coefficients with and without noise. (a) Wavelet coefficient with SNR 2 dB. (b) Wavelet coefficient with SNR 10 dB. (c) Denoising of the wavelet coefficient with SNR 2 dB. (d) Denoising of the wavelet coefficient with SNR 10 dB.

The middle point of the beam is taken as the symmetrical point to divide the element at both ends. After the element is divided, the end node of the first element at one end is taken as node 1 to the last element at the other end for node numbering in turn. Sixteen sensors were used for data acquisition. Point 1 is taken as the reference point, and the sensors are arranged on the central axis of the upper surface of the beam according to the node number successively from point 1, as shown in Figures 28(a) and 28(b), which show the schematic diagram of node numbering and sensor layout of scenario 1 in Table 3. The node numbering rule and sensor arrangement rule of scenario 2 are the same as those of scenario 1. The data collected are processed by the DH5922D analysis system. In Table 3, damage depth d is calculated according to the following equation:

$$(1-\gamma)I = I_i = \frac{1}{12}b(h-d)^3, \tag{21}$$

where I_i is the moment of inertia of the damaged section.

7.1. Experimental Results. Figure 30shows the wavelet coefficient graph of the modal data of the damaged steel beam. The prominent position of the wavelet coefficient is the singularity, which corresponds to the damage location of the beam. Due to the interference of the surrounding measurement noise in the experiment, after a certain amount of data denoising, larger singular values occur in the damage points, and there are also smaller singular values in other elements without damage. In addition, the damage information of element 12 in scenario 2 is covered by noise, which indicates that the damage information is easily affected by noise in the microdamage identification experiment.

Since scenario 1 is included in scenario 2, 0.8PSO, GA, BA, and IPSO are used to calculate the damage severity of the beam in scenario 2. As the data are polluted by noise, the minimum errors of IPSO, 0.8PSO, GA, and BA in identifying the damage severity of structures are 1.423%, 2.214%, 1.636%, and 1.572%, respectively, after denoising by the denoising tool in the MATLAB wavelet toolbox.

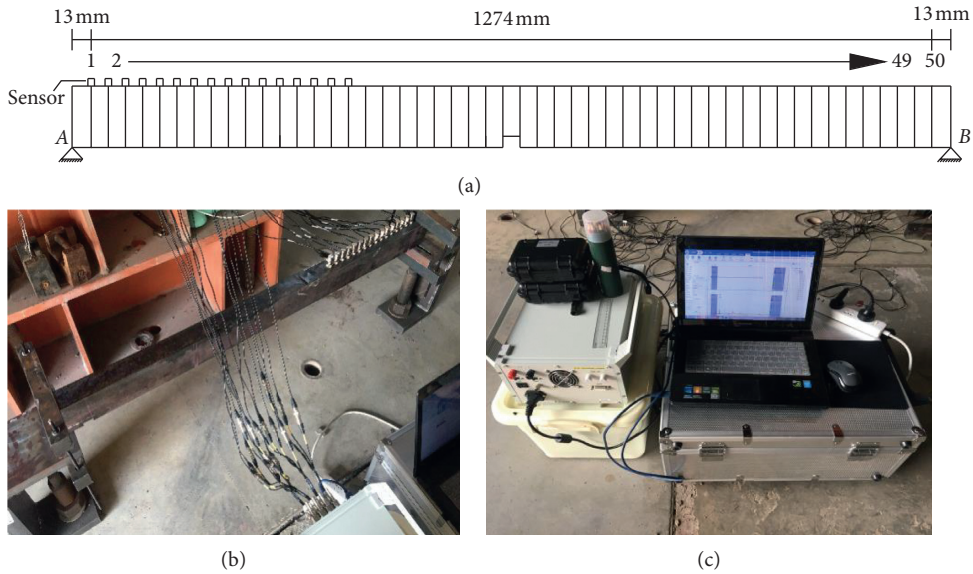

Figure 28: Experimental device layout. (a) Sensor layout. (b) Experimental beam. (c) Experimental equipment.

Figure 29: Damage setting.

Table 3: Details of experiment scenarios.

Scenarios	Element quantities	Element size (mm)	Length (mm)	Damage element	Damage severity (γ) (%)	Damage depth (d) (mm)
1	49	26	1274	25	20	5.7
				12	4	1.1
2	43	26	1118	25	20	5.7
				38	10	2.8

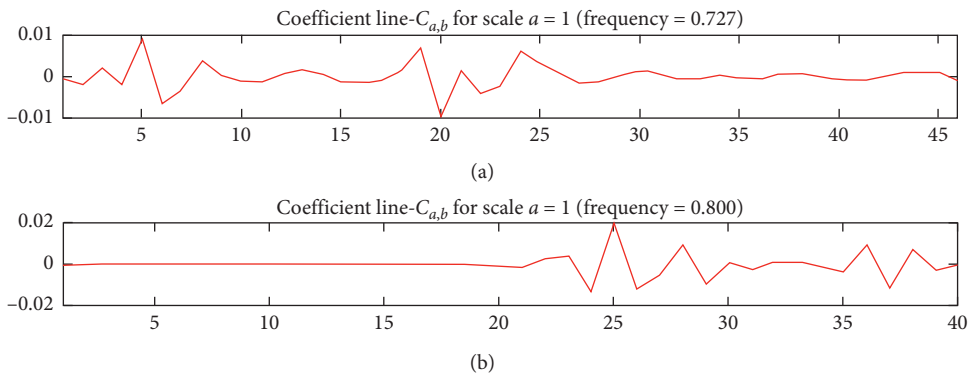

Figure 30: Experimental wavelet coefficients. (a) Wavelet coefficient of scenario 1. (b) Wavelet coefficient of scenario 2.

Table 4: Calculation results of h_i based on IPSO calculation results.

	$\gamma = 4\%$		$\gamma = 20\%$		$\gamma = 10\%$	
	h_i (mm)	$(h - h_i)/h$	h_i (mm)	$(h - h_i)/h$	h_i (mm)	$(h - h_i)/h$
1	78.5272	0.01841	73.0311	0.08711	76.5242	0.04345
2	78.5244	0.01844	73.0215	0.08723	76.5478	0.04315
3	78.5266	0.01842	73.0228	0.08722	76.5473	0.04316
4	78.5247	0.01844	73.0176	0.08728	76.5481	0.04315
5	78.5294	0.01838	73.0199	0.08725	76.5356	0.04330
6	78.5252	0.01843	73.0228	0.08722	76.5429	0.04321
7	78.5219	0.01848	73.0272	0.08716	76.5484	0.04314
8	78.5230	0.01846	73.0148	0.08732	76.5365	0.04329
9	78.5264	0.01842	73.0176	0.08728	76.5496	0.04313
10	78.5269	0.01841	73.0237	0.08720	76.5330	0.04334

According to the identification results of the damage severity of the fixed beam, the damage severity calculated by IPSO in scenario 2 was used for reverse calculation to obtain the height h_i of the damage section. The calculation equation of h_i is shown in equation (22), and the calculation results are shown in Table 4. Table 4 shows that the error of the height h_i of the damaged section is within 10%, which indicates that IPSO can effectively identify the structural damage severity.

$$(1 - \gamma)I = I_i = \frac{1}{12} b h_i^3. \tag{22}$$

By comparing experimental results with the numerical simulation results, the wavelet analysis in theory and experiment can effectively identify structural damage locations. IPSO in damage identification tests results in errors that are greater than those in the numerical simulation research, which is mainly due to the large influence of the environmental noise and smaller damage severity setting. Therefore, it is necessary to improve the denoising methods in future research. The experimental results show that IPSO can effectively identify the structural damage severity, and the calculation results have significant reference value.

8. Conclusion

Combining the advantages of wavelet analysis and IPSO, a structural microdamage identification method based on WIPSO is proposed in this study. In the first step, the microdamage location is accurately identified by the singularity and the maximum value of the wavelet coefficient, which is calculated by the strain mode of the structure. The results of the numerical simulation and experiment completely verify that wavelet coefficients can quickly and accurately identify structural damage locations and that noise has little interference on the accuracy of identification. After the damage location is identified, IPSO can calculate the structural damage severity by MATLAB. In numerical simulation, IPSO, GA, BA, and 0.8PSO are used to identify the damage severity of the structure. By comparing the damage identification results of these four intelligent algorithms, we can see that IPSO could accurately identify the damage severity, and the identification efficiency and running performance surpass some mainstream algorithms. Moreover, IPSO does not end prematurely and fall into local optimization during damage severity identification in this study, which indicated that IPSO is effective in improving the calculation method of inertia weight. Through two scenarios' experiments of fixed beam, the results show as the following: (1) WIPSO can easily and accurately identify the structural damage, (2) the wavelet coefficient as a damage index is intuitionistic and has antinoise performance, (3) the improvement of IPSO on the calculation method of inertia weight is effective, which improves the accuracy and efficiency of IPSO in identifying the structural damage, and(4) deviation exists in the identification of damage severity by WIPSO with the high influence of environmental noise, but the damage identification result is still of great value.

The proposed method shows great potential in theory and experiment; however, in application, the beam damage cannot be entirely transfixion damage along the thickness direction. Additionally, the damage severity is not always the same as the damage severity determined in the experiment. In a future study, we need to reduce the crack width and carry out damage experiments on nonuniform crack identification. The damage severity identification result is not ideal with the large environmental noise effect in the experiment, which indicates that further research involving effectively removing the noise is necessary. The above problems are practical problems that require further study so that WIPSO can be reliably applied to actual structures.

Data Availability

The data used to support the findings of this study are available from the corresponding author upon request. The IPSO codes are available from the provided network address: https://pan.baidu.com/s/1RlllyawBdSQg-zXKgQKaYw, extraction code: 2f2i.

Conflicts of Interest

The authors declare that they have no conflicts of interest regarding the publication of this paper.

Acknowledgments

This study was financially supported by the National Natural Science Foundation of China (no. 51378079).

References

[1] S. W. Doebling, C. R. Farrar, and M. B. Prime, "A summary review of vibration-based damage identification methods," *The Shock and Vibration Digest*, vol. 30, no. 2, pp. 91–105, 1998.

[2] W. Fan and P. Qiao, "Vibration-based damage identification methods: a review and comparative study," *Structural Health Monitoring*, vol. 10, no. 1, pp. 83–111, 2011.

[3] C. Zhang, L. Cheng, J. Qiu, H. Ji, and J. Ji, "Structural damage detections based on a general vibration model identification approach," *Mechanical Systems and Signal Processing*, vol. 123, pp. 316–332, 2019.

[4] H. Ji, J. V. A. dos Santos, and A. Katunin, "Identification of material properties of a laminated plate from measurements of natural frequencies and modal rotations," *Procedia Structural Integrity*, vol. 17, pp. 971–978, 2019.

[5] E. P. Carden and P. Fanning, "Vibration based condition monitoring: a review," *Structural Health Monitoring: An International Journal*, vol. 3, no. 4, pp. 355–377, 2004.

[6] Y. J. Yan, L. Cheng, Z. Y. Wu, and L. H. Yam, "Development in vibration-based structural damage detection technique," *Mechanical Systems and Signal Processing*, vol. 21, no. 5, pp. 2198–2211, 2007.

[7] Z. Y. Yam, S. S. Law, and L. M. Zhang, "Structural damage localization from modal strain energy change," *Journal of Sound and Vibration*, vol. 218, no. 5, pp. 825–844, 1998.

[8] S. S. Law, Z. Y. Shi, and L. M. Zhang, "Structural damage detection from incomplete and Noisy modal test data," *Journal of Engineering Mechanics*, vol. 124, no. 11, pp. 1280–1288, 1998.

[9] L. Y. Yam, T. P. Leung, D. B. Li, and K. Z. Xue, "Theoretical and experimental study of modal strain analysis," *Journal of Sound and Vibration*, vol. 191, no. 2, pp. 251–260, 1996.

[10] H. Guan and V. M. Karbhari, "Improved damage detection method based on element modal strain damage index using sparse measurement," *Journal of Sound and Vibration*, vol. 309, no. 3–5, pp. 465–494, 2008.

[11] Z.-D. Xu and K.-Y. Wu, "Damage detection for space truss structures based on strain mode under ambient excitation," *Journal of Engineering Mechanics*, vol. 138, no. 10, pp. 1215–1223, 2012.

[12] S. Wu, J. Zhou, S. Rui, and Q. Fei, "Reformulation of elemental modal strain energy method based on strain modes for structural damage detection," *Advances in Structural Engineering*, vol. 20, no. 6, pp. 896–905, 2017.

[13] D. C. Robertson, O. I. Camps, J. S. Mayer, and W. B. Gish, "Wavelets and electromagnetic power system transients," *IEEE Transactions on Power Delivery*, vol. 11, no. 2, pp. 1050–1058, 1996.

[14] Q. Cheng-Zhong and L. Xu-Wei, "Damage identification for transmission towers based on HHT," *Energy Procedia*, vol. 17, pp. 1390–1394, 2012.

[15] Z. K. Peng, P. W. Tse, and F. L. Chu, "An improved Hilbert-Huang transform and its application in vibration signal analysis," *Journal of Sound and Vibration*, vol. 286, no. 1-2, pp. 187–205, 2005.

[16] B. H. Kim, T. Park, and G. Z. Voyiadjis, "Damage estimation on beam-like structures using the multi-resolution analysis," *International Journal of Solids & Structures*, vol. 43, no. 14, pp. 4238–4257, 2005.

[17] X. Jiang and S. Mahadevan, "Wavelet spectrum analysis approach to model validation of dynamic systems," *Mechanical Systems and Signal Processing*, vol. 25, no. 2, pp. 575–590, 2011.

[18] J.-C. Hong, Y. Y. Kim, H. C. Lee, and Y. W. Lee, "Damage detection using the Lipschitz exponent estimated by the wavelet transform: applications to vibration modes of a beam," *International Journal of Solids and Structures*, vol. 39, no. 7, pp. 1803–1816, 2002.

[19] M. Rucka and K. Wilde, "Application of continuous wavelet transform in vibration based damage detection method for beams and plates," *Journal of Sound and Vibration*, vol. 297, no. 3–5, pp. 536–550, 2006.

[20] J. Zhou and Z. Li, "Damage detection based on vibration for composite sandwich panels with truss core," *Composite Structures*, vol. 229, Article ID 111376, 2019.

[21] C. Yang and S. O. Oyadiji, "Damage detection using modal frequency curve and squared residual wavelet coefficients-based damage indicator," *Mechanical Systems and Signal Processing*, vol. 83, pp. 385–405, 2017.

[22] S. S. Patel, A. P. Chourasia, S. K. Panigrahi, J. Parashar, N. Parvez, and M. Kumar, "Damage identification of RC structures using wavelet transformation," *Procedia Engineering*, vol. 144, pp. 336–342, 2016.

[23] R. Parashar, S. Rucevskis, M. Wesolowski, and A. Chate, "Experimental structural damage localization in beam structure using spatial continuous wavelet transform and mode shape curvature methods," *Measurement*, vol. 102, pp. 253–270, 2017.

[24] H. Gökdağ and O. Kopmaz, "A new damage detection approach for beam-type structures based on the combination of continuous and discrete wavelet transforms," *Journal of Sound and Vibration*, vol. 324, no. 3–5, pp. 1158–1180, 2009.

[25] M. Solís, M. Algaba, and P. Galvín, "Continuous wavelet analysis of mode shapes differences for damage detection," *Mechanical Systems and Signal Processing*, vol. 40, no. 2, pp. 645–666, 2013.

[26] W.-Y. He, S. Zhu, and W.-X. Ren, "Two-phase damage detection of beam structures under moving load using multi-scale wavelet signal processing and wavelet finite element model," *Applied Mathematical Modelling*, vol. 66, pp. 728–744, 2019.

[27] A. Mojtahedi, M. A. Lotfollahi Yaghin, Y. Hassanzadeh, F. Abbasidoust, M. M. Ettefagh, and M. H. Aminfar, "A robust damage detection method developed for offshore jacket platforms using modified artificial immune system algorithm," *China Ocean Engineering*, vol. 26, no. 3, pp. 379–395, 2012.

[28] M. Silva, A. Santos, E. Figueiredo, R. Santos, C. Sales, and J. C. W. A. Costa, "A novel unsupervised approach based on a genetic algorithm for structural damage detection in bridges," *Engineering Applications of Artificial Intelligence*, vol. 52, pp. 168–180, 2016.

[29] S. Tiachacht, A. Bouazzouni, S. Khatir, M. Abdel Wahab, A. Behtani, and R. Capozucca, "Damage assessment in structures using combination of a modified Cornwell indicator and genetic algorithm," *Engineering Structures*, vol. 177, pp. 421–430, 2018.

[30] H. Tran-Ngoc, S. Khatir, G. De Roeck et al., "Model updating for Nam O bridge using particle swarm optimization algorithm and genetic algorithm," *Sensors*, vol. 18, no. 12, 2018.

[31] S. Hakim, H. A. Razak, and S. Ravanfar, "Ensemble neural networks for structural damage identification using modal data," *International Journal of Damage Mechanics*, vol. 25, no. 3, pp. 400–430, 2016.

[32] M. Nakamura, S. F. Masri, A. G. Chassiakos et al., "Neural network approach to damage detection in a building from ambient vibration measurements," *Proceedings of SPIE*, vol. 33, no. 3, pp. 126–137, 1998.

[33] N. B. Guedria, "An accelerated differential evolution algorithm with new operators for multi-damage detection in plate-like structures," *Applied Mathematical Modelling*, vol. 80, pp. 366–383, 2020.

[34] M. Nobahari, M. R. Ghasemi, and N. Shabakhty, "A fast and robust method for damage detection of truss structures," *Applied Mathematical Modelling*, vol. 68, pp. 368–382, 2019.

[35] S. Chatterjee, S. Sarkar, S. Hore, N. Dey, A. S. Ashour, and V. E. Balas, "Particle swarm optimization trained neural network for structural failure prediction of multistoried RC buildings," *Neural Computing and Applications*, vol. 28, no. 8, pp. 2005–2016, 2017.

[36] Y. Zhao, Q. Yan, Z. Yang, X. Yu, and B. Jia, "A novel artificial bee colony algorithm for structural damage detection," *Advances in Civil Engineering*, vol. 2020, Article ID 3743089, 21 pages, 2020.

[37] Y. B. Chen, J. G. Han, D. Q. Yang et al., "Wavelet-based modal parameter identification through measurements for damage detection," *Key Engineering Materials*, vol. 353, pp. 1195–1198, 2007.

[38] A. R. M. Rao and K. Lakshmi, "Damage diagnostic technique combining POD with time-frequency analysis and dynamic quantum PSO," *Meccanica*, vol. 50, no. 6, pp. 1551–1578, 2015.

[39] D. Q. Guan, T. Jun, and H. Tao, "The method of structural damage identification by ACO algorithm and wavelet theory," *Advance in Intelligent Systems Research*, vol. 133, pp. 94–97, 2016.

[40] D. Q. Guan, J. Li, and J. Chen, "Optimization method of wavelet neural network for suspension bridge damage identification," *Advances in Intelligent Systems Research*, vol. 133, pp. 194–197, 2016.

[41] D. Q. Guan, D. Luo, and R. Li, "Damage identification method of suspension bridge structure based on wavelet-artificial immune algorithm," in *Proceedings of the 5th International Conference on Civil Engineering and Transportation*, Guangzhou, China, 2015.

[42] S. A. Ravanfar, H. A. Razak, Z. Ismail, and S. J. S. Hakim, "A two-step damage identification approach for beam structures based on wavelet transform and genetic algorithm," *Meccanica*, vol. 51, no. 3, pp. 635–653, 2016.

[43] J. Kennedy and R. C. Eberhart, "A discrete binary version of the particle swarm algorithm," in *Proceedings of the IEEE International Conference on Systems, Man, and Cybernetics. Computational Cybernetics and Simulation*, vol. 5, pp. 4104–4108, Orlando, FL, USA, October 1997.

[44] H. M. Van and H. J. Kang, "Bearing defect classification based on individual wavelet local Fisher discriminant analysis with particle swarm optimization," *IEEE Transactions on Industrial Informatics*, vol. 12, no. 1, pp. 124–135, 2015.

[45] F. Jiang, H. Xia, Q. Anh Tran, Q. Minh Ha, N. Quang Tran, and J. Hu, "A new binary hybrid particle swarm optimization with wavelet mutation," *Knowledge-Based Systems*, vol. 130, pp. 90–101, 2017.

[46] Y. Chen, L. Li, J. Xiao, Y. Yang, J. Liang, and T. Li, "Particle swarm optimizer with crossover operation," *Engineering Applications of Artificial Intelligence*, vol. 70, pp. 159–169, 2018.

[47] H. Tran-Ngoc, L. He, and E. Reynders, "An efficient approach to model updating for a multispan railway bridge using orthogonal diagonalization combined with improved particle swarm optimization," *Journal of Sound and Vibration*, vol. 476, Article ID 115315, 2020.

[48] S. Khatir, S. Tiachacht, C.-L. Thanh, T. Q. Bui, and M. A. Wahab, "Damage assessment in composite laminates using ANN-PSO-IGA and Cornwell indicator," *Composite Structures*, vol. 230, Article ID 111509, 2019.

[49] X. Ge, Y. J. Yan, and H. G. Chen, "A damage detection method: CMSE combined with Niche GA," *Advances in Composite Materials and Structures*, vol. 334, pp. 929–932, 2007.

[50] R. Zenzen, I. Belaidi, S. Khatir, and M. A. Wahab, "A damage identification technique for beam-like and truss structures based on FRF and Bat algorithm," *Comptes Rendus Mécanique*, vol. 346, no. 12, pp. 1253–1266, 2018.